Available online at www.sciencedirect.com
SCIENCE DIRECT
Sensors and Actuators A 125 (2006) 170–177
SENSORS AND ACTUATORS A PHYSICAL
www.elsevier.com/locate/sna

Thin film temperature sensor for real-time measurement of electrolyte temperature in a polymer electrolyte fuel cell

Suhao He [a], Matthew M. Mench [a], Srinivas Tadigadapa [b,*]

[a] *Fuel Cell Dynamic and Diagnostic Laboratory, and Department of Mechanical and Nuclear Engineering, The Pennsylvania State University, University Park, PA 16802, USA*
[b] *Department of Electrical Engineering, The Pennsylvania State University, 111J EE West Bldg., University Park, PA 16802, USA*

Received 12 January 2005; received in revised form 25 May 2005; accepted 25 May 2005
Available online 15 August 2005

Abstract

This paper describes a technique for the measurement of the electrolyte temperature in an operating polymer electrolyte fuel cell (PEFC). A patterned thin film gold thermistor embedded in a 16 μm thick parylene film was laminated in the Nafion® electrolyte layer for in situ temperature measurements. Experimental results show that the sensor has a linear response of $(3.03 \pm 0.09) \times 10^{-3}\,^{\circ}\mathrm{C}^{-1}$ in the 20–100 °C temperature range and is robust enough to withstand the electrolyte expansion forces that occur during water uptake. An electrolyte temperature increase of 1.5 °C was observed in real-time when operating the fuel cell at 0.2 V and a current density of 0.19 A/cm^2. The temperature sensitivity of the present sensor is in an order of magnitude better than the conventional micro-thermocouples that have been reported. Additionally, use of micro-fabrication techniques allows for an accurate placement of the temperature sensor within the fuel cell. Simulation results show that the sensor has no significant effect on the local temperature distribution.

Keywords: Thin film thermistor; MEMS; Microstructure; Polymer electrolyte fuel cell; Solid polymer electrolyte; Temperature measurement

1. Introduction

Temperature measurement of an operating polymer electrolyte fuel cell (PEFC) is critical to understand for cold start, water balance, and degradation. This paper describes the development of a thin film thermal sensor for the real-time measurement of temperature in an operating PEFC. A patterned thin film gold thermistor embedded in a 16 μm thick parylene film was laminated in the Nafion® electrolyte layer for in situ temperature measurements.

Temperature distribution in a PEFC is of critical importance because of the close ties with water management at the PEFC operating temperature of 80 °C. The electrolyte, Nafion® membrane, has to be saturated with water to conduct protons, but too much water can lead to local flooding. With poor thermal management, short-term effects will be a performance loss due to either membrane dry-out or diffusion media flooding, and long-term effects will be the sulfonate group decomposition due to the high temperature, which could increase the fuel crossover rate through the electrolyte, thus degrading the cell performance. At an extreme case, pinholes formed lead to membrane failure [1,2]. Thermal management is also important for cold start cycling, when residual water freeze–thaw could degrade the cell performance [3]. Researchers have been engaged in real-time temperature measurement in a PEFC for some time, especially the electrolyte temperature. A review of various methods for achieving temperature distribution, including infrared technology is given by Wang et al. [4]. Vie and Kjelstrup [5]

* Corresponding author. Tel.: +1 814 865 2730; fax: +1 814 865 7065.
E-mail address: sat10@psu.edu (S. Tadigadapa).

0924-4247/$ – see front matter © 2005 Elsevier B.V. All rights reserved.
doi:10.1016/j.sna.2005.05.021

placed a millimeter sized thermocouple at various locations on a membrane electrolyte assembly (MEA). Mench et al. and Burford [6,7] laminated eight 50 μm thermocouples directly into two Nafion® 111 membranes. With this method, placement of the thermocouples in exact positions is difficult. Also, possible interference with local temperature distribution has to be considered, since the thermocouple wire diameter is equivalent to the electrolyte membrane thickness.

In order to achieve higher spatial resolution and sensitivity, further reduction in the sensor size is required. Thin film thermal sensors have been developed for an array of applications. Most of them are fabricated on solid substrates, such as silicon and glass. Brunco et al. [8] used lithographic technology to fabricate thermistors to measure the interface temperature between a polyimide film and a quartz substrate to study laser-induced heating and ablation. Debey et al. [9] also used lithographic technology to fabricate thin film thermocouples with 10 measurement points in 2 mm on the polyimide and ceramics substrates. Krishnan et al. [10] fabricated thin film thermocouples on flexible polymer and paper substrates by thermal evaporation to measure the properties of thin film. However, the temperature measurements for PEFC application have to be performed on a Nafion® (E.I. du Pont de Nemours) substrate, a perfluorinated polymer that contains connected islands of sulfonic ionic functional groups, and has a linear expansion of 10 to 50% of the relative humidity to water saturated fully at 23 °C [11]. Therefore, one critical challenge is to design a sensor that will withstand the stretching force during the electrolyte water uptake. Such a sensor should work at any environment similar to a PEFC: acidic, electrochemical, and with unstable polymer substrate.

To protect thin film sensors from degradation, researchers have utilized Al_2O_3, TaO, borosilicate, and polymer materials as insulating films. Ruff and Kreider [12] emphasize the following properties for insulation application: adhesion, low electrical conductivity, high strength, and hardness. Polymer insulator and encapsulating thin films, especially parylene, has been widely applied in several thermal microsensors. In many of these applications the polymer film is used for the protection of thin film thermistors, thermopiles, and microheaters from degradation in the environment. Applications of such sensors include thermal sensors [13,14], flow sensor [15], chemical sensor [16,17], stress sensor [18], and other applications [19,20]. The most important outcome of encapsulating the thin film micro-fabricated thermistors in parylene, as demonstrated in this paper, is the successful demonstration of a thin film temperature sensor in the fuel cell environment, which poses a very difficult problem due to the substrate undergoing a very large expansion upon exposure to the conditions. Wolgemuth [21] has listed the desirable properties of parylene, which include a simple vapor deposition process capable of producing uniform coating, stability, and low residual stress.

This paper describes the fabrication process and the performance of a thin film based temperature sensor for monitoring the temperature in a fuel cell during its operation. The paper also includes a modeling analysis of sensor interference with local temperature distribution.

2. Design and fabrication process

Fig. 1 depicts the sensor design layout that was used. The 5 cm^2 fuel cell flow channels are in the middle, as represented by dashed lines. They are composed of three parallel gas channels. Protons transport through this area of the Nafion® membrane from the fuel cell anode to the cathode. Reaction inefficiency, entropy change, and joule heating result in an increase in the temperature of the Nafion® membrane. To measure the membrane temperature at different locations of the flow channels, the temperature sensors are located precisely within the flow channel area and connection legs are placed outside the area.

The design uses thermistors to directly measure the temperature of the PEFC reactant flow inlet and outlet. Parylene layers are used to protect the sensor from the stretching force of the Nafion® membrane. As shown in Fig. 1, the closed lines surrounding the sensor set are the parylene cover area.

The fabrication process includes two major steps: one is to fabricate the sensor on the Nafion® membrane and the other is to integrate the Nafion® membrane with the sensor into a fuel cell. The fabrication began with cleaning of the Nafion® 112 membrane (50 μm thick), using 5 wt.% H_2O_2 at 80 °C for an hour and washing with deionized water for half an hour, followed by the same process with 1 M H_2SO_4 and drying the membrane. An 8 μm thick parylene layer was deposited on the Nafion® membrane, using a metal shadow mask with rubber seals. This was followed by the deposition of the thermistor metal, a 150 Å Cr/2000 Å Au layer, accomplished by using e-beam evaporation while the patterns were transferred by a shadow mask. Another 8 μm thick parylene layer was deposited to cover the entire sensor area, except the legs for the connection wire bonding. Then, the sample was laminated with another clean Nafion® 112 membrane and the two electrodes at 125 °C and 100 kgf/cm^2 for 3 min.

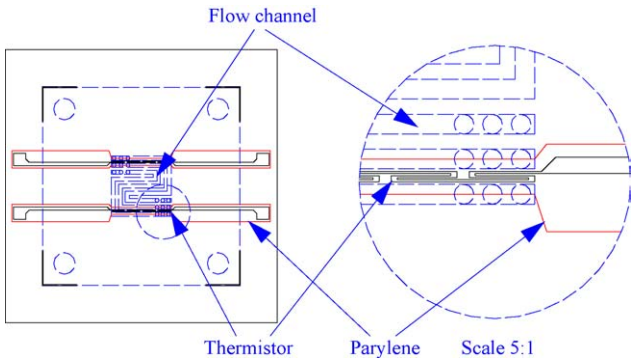

Fig. 1. Temperature sensor design (the right figure is the enlarged view).

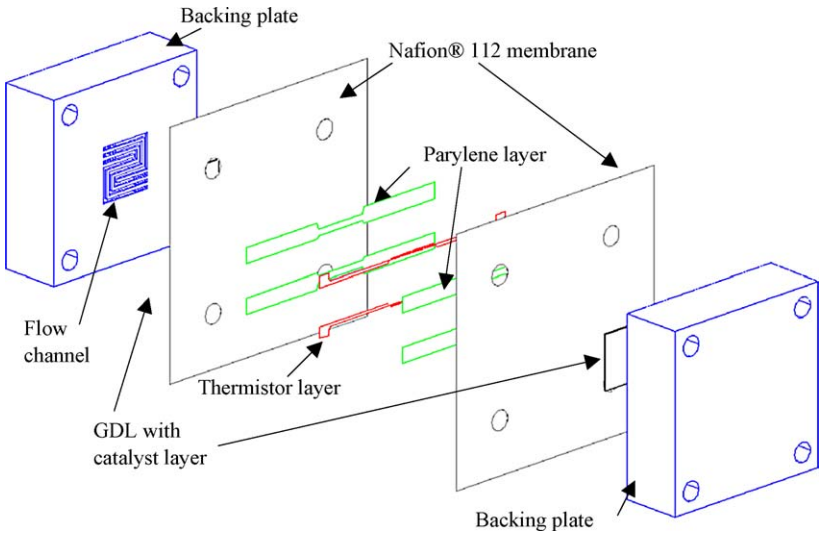

Fig. 2. Sensor set-up in a fuel cell.

A 10 μm thick catalyst layer was sprayed on the gas diffusion layer (GDL) using an airbrush. The catalyst was prepared using E-TEK® 40 wt.% carbon-supported Pt and Nafion® 5 wt.% solution. The Pt loading was 0.3 mg/cm^2. The GDL used was E-TEK® 400 μm thick carbon cloth. Fig. 2 shows the position of each part in the fuel cell.

3. Thermal analysis

The two Nafion® 112 membranes are 102 μm thick, while the parylene insulating layer is 16 μm thick. It is necessary to study whether the parylene layer influences the local temperature distribution. Divisek [22] gave a review on the current status of the research on low temperature fuel cell heat transfer.

A simplified 2D heat conduction model was set up to calculate the heat transport process with more details shown in He et al. [23]. A major assumption for the model is that the parylene layer is small enough and it will not block proton transport. Also, mass transfer and two-phase porous flow has not been considered and the whole water product exists in vapor phase. Many more detailed fuel cell models can be found in literature [24–29].

Typically, a PEFC consists of two bipolar plates, flow channels, GDLs, electrodes, and electrolyte membrane, as shown in Fig. 2. Heat is generated in the electrodes and the electrolyte and dissipated through the GDLs, flow channels, and backing plates. Isothermal boundary conditions (BCs) are used at the outside walls of the backing plates and symmetric BCs in the other walls, except for the flow channel walls with forced convection BCs [30].

The operating voltage of a hydrogen fuel cell V_{cell} at a current density i can be calculated by reversible open circuit voltage (OCV) E^0 from Nernst equation and ohmic activation, and mass voltage loss η at the cell assembly [31], which can be written as

$$\begin{aligned} V_{\text{cell}} &= E^0 - \eta_{\text{Ohmic,e}} - \eta_{\text{Ohmic,a}} - \eta_{\text{Ohmic,c}} - \eta_{\text{Activation,a}} \\ &\quad - |\eta_{\text{Activation,c}}| - \eta_{\text{Mass,a}} - \eta_{\text{Mass,c}} \\ &= E^0 - (i+i_{\text{n}})r_{\text{e}} - (i+i_{\text{n}})r_{\text{a}} - (i+i_{\text{n}})r_{\text{c}} \\ &\quad - \left(\frac{RT}{2F}\right)\frac{i+i_{\text{n}}}{i_{0,\text{a}}} - \left(\frac{RT}{\alpha_{\text{c}}F}\right)\ln\left[\frac{i+i_{\text{n}}}{i_{0,\text{c}}}\right] \\ &\quad + \left(\frac{RT}{2F}\right)\ln\left[1-\frac{i+i_{\text{n}}}{i_{\text{l,a}}}\right] + \left(\frac{RT}{4F}\right)\ln\left[1-\frac{i+i_{\text{n}}}{i_{\text{l,c}}}\right] \end{aligned} \tag{1}$$

where i_{n} is the crossover current; $i_{0,\text{a}}$ and $i_{0,\text{c}}$ the exchange current densities at the anode and the cathode; $i_{\text{l,a}}$ and $i_{\text{l,c}}$ the limiting current densities at the anode and the cathode; α_{c} the cathodic charge transfer coefficient; r_{e}, r_{a}, and r_{c} the resistance of the electrolyte (ionic), the anode, and the cathode; T the temperature; R the gas constant; and F the Faraday's constant. The expression for $\eta_{\text{Activation,c}}$ is valid when $(i+i_{\text{n}}) > i_{0,\text{c}}$.

The 2D steady energy equation is expressed as

$$\frac{\partial^2 T}{\partial x^2} + \frac{\partial^2 T}{\partial y^2} + \frac{\dot{q}'''}{k} = 0 \tag{2}$$

Heat is generated by three ways: (1) activation polarization heat, generated by the electrochemical reactions taking place in the electrodes; (2) ohmic heat, generated by the current going through the membrane and the catalyst layers; (3) Peltier heat generated by the entropy change. Thus, most of the heat is generated within the very thin membrane and catalyst layers. The heat source in the anode $\dot{q}'''_{\text{a}}$ is

$$\dot{q}'''_{\text{a}} = \frac{(i+i_{\text{n}})(\eta_{\text{Ohmic,a}} + \eta_{\text{Activation,a}} + \eta_{\text{Mass,a}})}{\delta_{\text{a}}} + \dot{q}'''_{\text{peltier}} \tag{3}$$

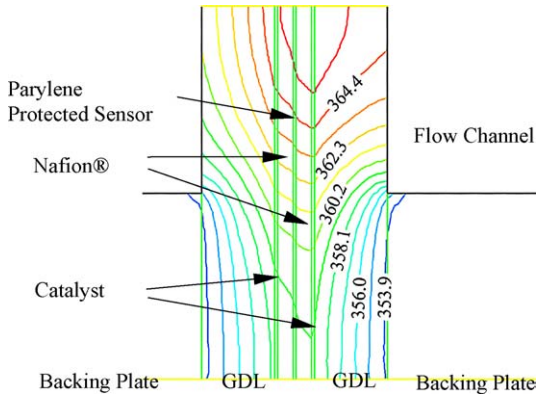

Fig. 3. Temperature contours for the case of 1 A/cm^2 and 10 μm thick parylene layer.

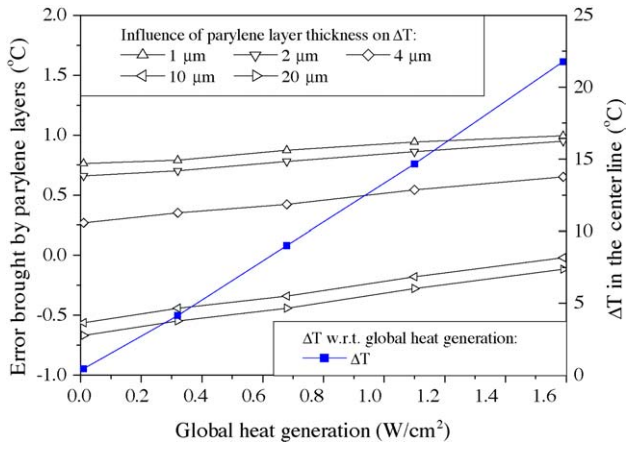

Fig. 4. Plot of the averaged temperature increase in the centerline and error brought by the parylene layer vs. global heat generation for different parylene layers thickness.

the heat source in the electrolyte $\dot{q}'''_e$ is

$$\dot{q}'''_e = \frac{(i + i_n)\eta_{Ohmic,e}}{\delta_e} \quad (4)$$

and the heat source in the cathode $\dot{q}'''_c$ is

$$\dot{q}'''_c = \frac{(i + i_n)(\eta_{Ohmic,c} + |\eta_{Activation,c}| + \eta_{Mass,c})}{\delta_c} + \dot{q}'''_{peltier} \quad (5)$$

The Peltier heat source is assumed to be evenly distributed in the anode and the cathode:

$$\dot{q}'''_{peltier} = \frac{(i + i_n)(-T\,\Delta S/nF)}{\delta_a + \delta_c} \quad (6)$$

ΔS is the entropy change of the global reaction. δ_a, δ_e, and δ_c are the thickness of the anode, the electrolyte, and the cathode.

Fig. 3 gives the temperature contours for a typical case of 1 A/cm^2 current density and 10 μm thick parylene layer, which shows that the temperature gradient concentrates in the MEA area. The calculated average temperature ΔT in the centerline of MEA, where the sensor is located, is 9 °C higher than the flow channel temperature. This temperature difference ΔT is influenced by the fuel cell operation conditions and component properties, especially the GDL properties.

Dong et al. [32] indicated that ΔT is proportional to the global heat generation $\dot{q}''_{global}$, which is defined as

$$\dot{q}''_{global} = (i + i_n)(1.25 - V_{cell}) \quad (7)$$

Fig. 4 confirms the linear relation. It also shows the error of ΔT brought by the parylene layer versus $\dot{q}''_{global}$ for different parylene layer thickness. There is only a minor temperature change caused by the insertion of parylene layer protected sensors, with absolute value less than 1 °C, though it could be significant for the case of low global heat generation.

4. Results and discussion

Initial attempts to deposit the thermistor metal directly on the Nafion® membrane were unsuccessful. The thin film metal became discontinuous very quickly during the swelling of the Nafion® membrane in water as shown in Fig. 5(a). Several approaches were attempted to resolve this issue. First, a polyethylene terephthalate (PET) film was deposited and patterned with the sensor thin film and then laminated with another PET(P) film. Then the P–P laminate was laminated between the two Nafion®(N) membranes to form an N–P–P–N laminate. Though this arrangement was able to resist the stretching force during hydration of the Nafion® membrane, Fig. 5(b) indicates that water still penetrated and damaged the sensor. Epotek® Epoxy 301 and acrylic adhesive were used to keep the PET membranes sealed, as shown in Fig. 5(c) and (d). Although we were able to achieve stable thermistors using these techniques, the advantages over using conventional macroscopic thermal sensors were lost, since the minimum thickness of the sensor set approached ~75 μm.

Since parylene is known to be hydrophobic, this material was used to embed the thermistor. Initially, the results seemed inconsistent, because a thin film protected by a 2 μm thick parylene layer showed cracks, as shown in Fig. 5(e), while another with 1 μm thick parylene layer did not, as shown in Fig. 5(f). It was later found that the robustness of the sensor depends on the parylene layer thickness and its ability to detach from the Nafion® membrane during water uptake. Whenever parylene was not subject to the stretching forces, the sensor remained intact. A sacrificial layer between the Nafion® layer and the parylene layer was used to promote successful delamination. A 15 nm Cr or Al layer as sacrificial layer and two 8 μm thick parylene layers were determined the best and repeatable combination to protect the embedded sensor.

Since the thermistors are not standard components, an ex situ calibration was determined. A standard K-type thermo-

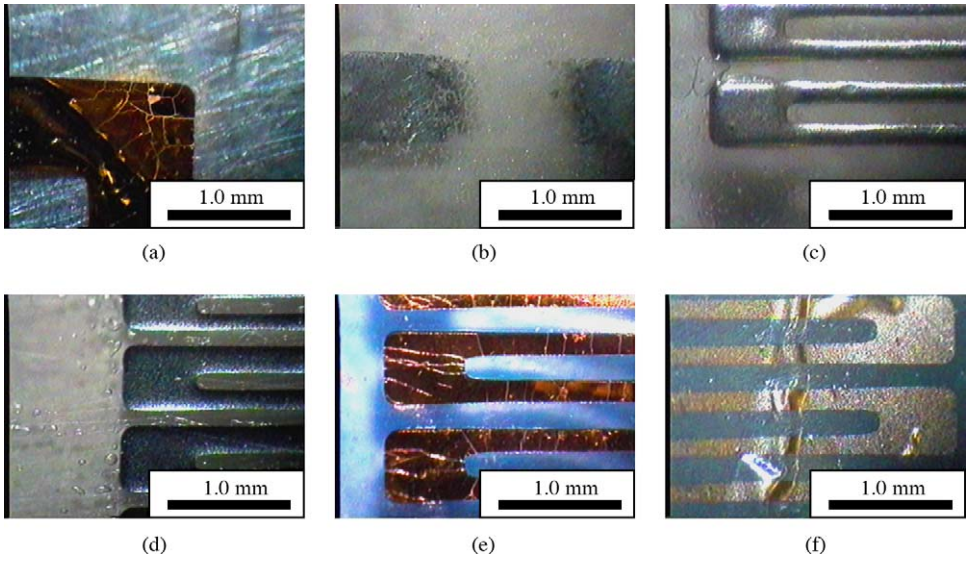

Fig. 5. Magnified view of thin film sensors: (a) cracks grow on sensor directly deposited on Nafion® membrane; (b) water can penetrate the N–P–P–N laminate and destroy the sensor; (c) N–P–P–N laminate with the aid of Epoxy® 301; (d) N–P–P–N laminate with the aid of acrylic adhesive; (e) cracks grow on sensor with 2 μm thick parylene protecting layer; and (f) sensor with 1 μm thick parylene protecting layer.

couple and the thin film thermistor were submerged in a water bath and kept in close proximity. The K-type thermocouple was connected to a FLUKE 52II thermometer and the thin film thermistor was connected to a FLUKE 8840A multimeter. The water bath was heated by a hot plate. Before calibrating, the water bath was boiled for few minutes to remove any air dissolved in the water and prevent the formation of two-phase flow below 100 °C, thus extending the stable range for calibration. The calibration was completed during the cooling-down process.

Calibration results are shown in Fig. 6, a plot of the thermistor resistance versus temperature during calibration. The curves show that the resistance has a linear dependence on temperature, and the slope remains constant even after 10 days, though the *y*-intercept shifts slightly, which is caused by the change in the bonding wires contact resistance. The

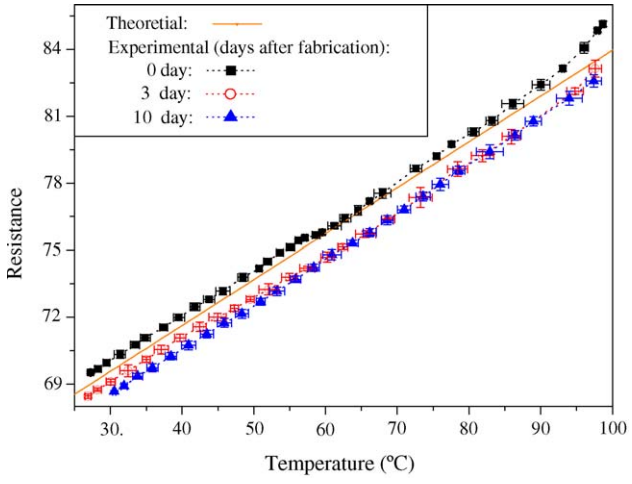

Fig. 6. Plot of thermistor resistance vs. temperature during ex situ calibration. The test was done at different days to check repeatability.

calibration measurement error is expected to be caused by the flow in the water bath, especially when the temperature approaches the boiling point, and to be less than 1 °C. The theoretical resistance in Fig. 6 is calculated as

$$R = R_{\text{leg}} + R_{25\,^\circ\text{C}}[1 + \gamma(T - 25)] \tag{8}$$

$R_{25\,^\circ\text{C}}$ is calculated by thermistor geometry, R_{leg} estimated, which includes the resistance of the leg and wires and contact resistance, and γ the temperature coefficient for the thin film metal used.

The ex situ calibration results were later confirmed with respect to linearity and durability by an in situ calibration in an operating fuel cell. For in situ conditions, the sensor output is still highly linear within the fuel cell operation temperature. There is also a similar *y*-intercept shift in the total resistance. The sensor is robust and the slope was constant after at least five cycles in 12 days. We expect the longer-term performance to be stable, since results from applications in semiconductor packaging industry [33] show that the parylene coating can help to release the strain force and extend solder lifetime significantly under thermal cycling conditions. By supplying nitrogen gas at T_1 to the fuel cell set-up until thermal equilibrium is reached, the resistance R_1 is measured. Then, the same steps are repeated at a temperature T_2, and R_2 is measured. So, the slope for the *R*–*T* curve is

$$S = \frac{R_2 - R_1}{T_2 - T_1} \tag{9}$$

When using the sensor, the temperature measured by the sensor will be

$$T = 25 + \frac{R - R_{25\,^\circ\text{C}}}{S} \tag{10}$$

where $R_{25\,^\circ\text{C}}$ is the resistance at 25 °C.

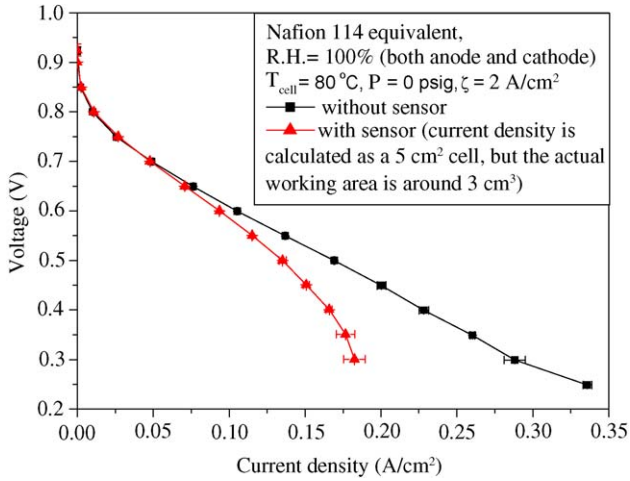

Fig. 7. Plot of the 5 cm^2 fuel cell performance with the sensor-MEA sandwich.

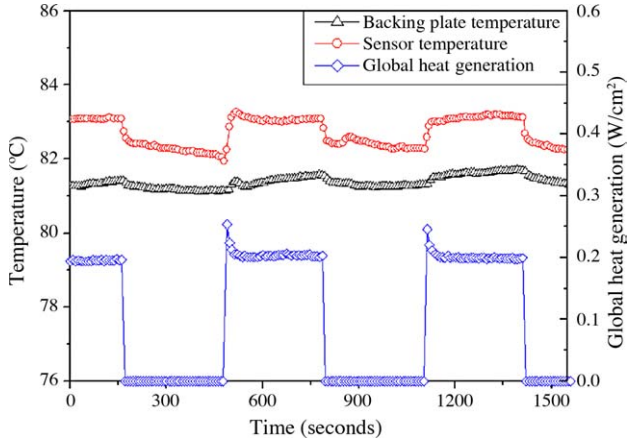

Fig. 9. Plot of fuel cell transient response measured by the sensor. The cell voltage was changed between OCV and 0.2 V every 5 min. The heat generation flux was around 0.2 W/cm^2 at 0.2 V.

The sensitivity of the sensor, $\Delta R/(R\,\Delta T)$, is calculated to be $(3.03 \pm 0.09) \times 10^{-3}\,°C^{-1}$ from the experimental results. There is 9% difference between $\Delta R/(R\,\Delta T)$ and the temperature coefficient of the resistance of pure gold (99.999+), $3.5 \times 10^{-3}\,°C^{-1}$ [34]. Here $\Delta R/(R\,\Delta T)$ was calculated based on the total resistance of the sensor and only the working part of the sensor is subject to temperature change. Also, the temperature coefficient of pure metal decreases sharply with increasing impurity or alloy content [35]. This sensitivity is in an order of magnitude better than the micro-thermocouples developed by the authors in previous study [6,7], with precise location control.

The performance of the fuel cell with embedded sensor was tested in 100% anode and cathode humidification at 80 °C and room pressure with a stoichiometry of 2 A/cm^2. The *V–i* curves are shown in Fig. 7. Since the parylene layer blocks almost 1/3 of the proton transport area for these small active area cells, the performance of the MEA with sensor is not as high as the one without sensor. However, these tests were conducted to demonstrate feasibility of using the sensor in fuel cells. Operation in large area cells with a much lower fraction of affected active area and high performance electrodes should yield nearly identical performance between cells with and without sensor.

Besides the thin film sensor, commercially available thermocouples were also inserted into the backing plates of the PEFC. Fig. 8(a) shows the fuel cell shutdown temperature response. The temperature of the electrolyte, measured by the sensor, followed exactly the same trend as backing the plate temperature change, as the cell cooled by natural convection. This type of test can also be used for in situ calibration. Fig. 8(b) shows the fuel cell start-up temperature response. Since cartridge heaters were working in the backing plates, the profile of the temperature followed the PID control. The electrolyte temperature was also influenced by inlet gas from the humidifiers. Temperature jumps can be seen from the figure, which represent inlet gas temperature jump.

Fig. 9 shows the fuel cell transient response measured by the sensor. The cell voltage was changed between the open circuit voltage and 0.2 V every 5 min. With this technique, the heat generation flux fluctuated between 0.2 W/cm^2 at 0.2 V and 0 W/cm^2 at OCV. The temperature jump is at least 1.5 °C. From calculation result in Fig. 4, the ΔT is around 2.5 °C and the error brought by parylene is around −0.5 °C for 16 μm thick parylene layer at 0.2 W/cm^2. They give an estimated sensor temperature of 2 °C. There is less than 0.5 °C difference between the theoretically estimated temperature and the measured one and this could be generated by the blockage of

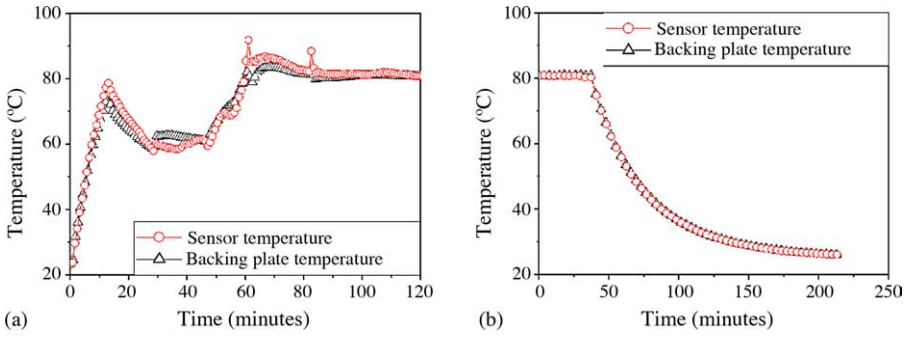

Fig. 8. Plot of fuel cell temperature response for (a) heat-up and (b) cool-down.

parylene on local proton transport, thus local heat generation is reduced.

It is the first report of a thin film thermistor integrated into a polymer electrolyte fuel cell for in situ temperature measurement. While the paper clearly demonstrates a path to make such temperature measurement, the current size of the sensor in relation to the fuel cell active area has resulted in an overall reduced performance of the fuel cell. By further minimizing the sensor size this method could produce a series of more practical sensors for fuel cell applications.

5. Conclusions

This paper describes the development of a thin film thermal sensor for application in an operating PEFC. The sensor set is around 16 μm thick and is fabricated using micro-fabrication techniques. By using a Nafion|Parylene |Sensor|Parylene|Nafion laminated structure we were able to protect the sensor from the electrolyte expansion forces. The thickness of the parylene stress insulation layer and the delamination of the parylene layer from the Nafion® membrane are keys to the survival of the sensor in PEFC environment.

Calibration results show that in the 20–100 °C temperature range the sensor has a linear response of $(3.03 \pm 0.09) \times 10^{-3}\,^{\circ}\mathrm{C}^{-1}$. Temperature sensitivity of the sensor is in an order of magnitude better than the micro-thermocouples developed in a previous study, with precise location control. Modeling results also show that the sensor has limited effects on the local temperature distribution.

Moreover, the thin film sensor has the potential to be further minimized using photolithography and etch technologies. Future work will be concentrated on the application of the sensor in a 50 cm^2 fuel cell with high performance electrodes to conduct steady state and dynamic heat transfer study.

Acknowledgements

Financial support of Hydrogen Energy Center (H_2E) and Material Research Institute (MRI) at Penn State is gratefully acknowledged.

References

[1] G. Hoogers, in: G. Hoogers (Ed.), Fuel Cell Technology Handbook, CRC Press, New York, 2003, pp. 1–27, Chapter 4.
[2] D.P. Wilkinson, J. St-Pierre, in: W. Vielstich, H.A. Gasteiger, A. Lamm (Eds.), Handbook of Fuel Cells, Fundamentals, Technology and Applications, vol. 3, John Wiley & Sons, New York, 2003, pp. 611–626, Chapter 47.
[3] E.-A. Cho, J.-J. Ko, H.Y. Ha, S.-A. Hong, K.-Y. Lee, T.-W. Lim, I.-H. Oh, Characteristics of the PEMFC repetitively brought to temperatures below 0 °C, J. Electrochem. Soc. 150 (2003) A1667–A1670.
[4] M.H. Wang, H. Guo, C.F. Ma, F. Ye, J. Yu, X. Liu, Y. Wang, C.Y. Wang, Temperature measurement technologies and their applications in the research of fuel cells, in: Proceedings of the First International Conference on Fuel Cell Science, Engineering and Technology, Fuel Cell Science, Engineering and Technology, Rochester, NY, USA, 21–23 April, 2003, pp. 95–100.
[5] P.J.S. Vie, S. Kjelstrup, Thermal conductivities from temperature profiles in the polymer electrolyte fuel cell, Electrochim. Acta 49 (2004) 1069–1077.
[6] M.M. Mench, D.J. Burford, T.W. Davis, In situ temperature distribution measurement in an operating polymer electrolyte fuel cell, in: Proceedings of 2003 ASME International Mechcanical Engineering Congress, Heat Transfer Division, Washington, DC, USA, 15–21 November, 2003, pp. 415–428.
[7] D.J. Burford, Real-time electrolyte temperature measurement in an operating polymer electrolyte membrane fuel cell, Master thesis, The Pennsylvania State University, University Park, 2004.
[8] D.P. Brunco, M.O. Thompson, C.E. Otis, P.M. Goodwin, Temperature measurements of polyimide during KrF excimer laser ablation, J. Appl. Phys. 72 (1992) 4344–4350.
[9] D. Debey, R. Bluhm, N. Habets, H. Kurz, Fabrication of planar thermocouples for real-time measurements of temperature profiles in polymer melts, Sens. Actuators A 58 (1997) 179–184.
[10] S. Krishnan, S.V. Babu, R. Bowen, L.P. Demejo, H. Osterhoudt, D.S. Rimai, Use of thin film thermocouples to determine the thermal conductivity and Young's modulus of coatings and interfaces, J. Adhes. 42 (1993) 103–112.
[11] E.I. du Pont de Nemours and Company, DuPont™ Nafion® PFSA Membrane N-112, NE-1135, N-115, N-117, NE-1110 perfluorosulfonic acid polymer, 2002, http://www.dupont.com/fuelcells/pdf/nae101.pdf.
[12] A.W. Ruff, K.G. Kreider, Deposited thin film wear sensors: materials and design, Wear 203–204 (1997) 187–195.
[13] Y. Zhang, S. Tadigadapa, Thermal characterization of liquids and polymer thin films using a microcalorimeter, Appl. Phys. Lett. 86 (2005) 1–3.
[14] K. Kurabayashi, M. Asheghi, M. Touzelbaev, K.E. Goodson, Measurement of the thermal conductivity anisotropy in polyimide films, J. MEMS Syst. 8 (1999) 180–191.
[15] A. Huang, J. Lew, Y. Xu, Y.-C. Tai, C.-M. Ho, Microsensors and actuators for macrofluidic control, IEEE Sens. J. 4 (2004) 494–502.
[16] A. Koll, A. Schaufelbuhl, N. Scheeberger, U. Munch, O. Brand, H. Baltes, C. Menolfi, Q. Huang, Micromachined CMOS calorimetric chemical sensor with on-chip low noise amplifier, in: Proceedings of the 1999 12th IEEE International Conference on Micro Electro Mechanical Systems, MEMS, Orlando, FL, USA, 17–21 January, 1999, pp. 547–551.
[17] M. Aslam, J.V. Hatfield, Fabrication of thin film microheater for gas sensors on polyimide membrane, in: Proceedings of the Second International Conference on Sensors: IEEE Sensors 2003, Toronto, Ont., Canada, 22–24 October, 2003, pp. 389–392.
[18] Z. Fan, J.M. Engel, J. Chen, C. Liu, Parylene surface-micromachined membranes for sensor applications, J. MEMS Syst. 13 (2004) 484–490.
[19] E. Kim, M.N. Niu, Piezoelectric bimorph microphone built on micromachined parylene diaphragm, J. MEMS Syst. 12 (2003) 892–898.
[20] V. Podzorov, V.M. Pudalov, M.E. Gershenson, Field-effect transistors on rubrene single crystals with parylene gate insulator, Appl. Phys. Lett. 82 (2003) 1739–1741.
[21] L. Wolgemuth, Accessing the performance and suitability of parylene coating, Med. Device Diagnostic Ind. 8 (2000) 42–51.
[22] J. Divisek, in: W. Vielstich, A. Lamm, H.A. Gasteiger (Eds.), Handbook of Fuel Cell, Fundamentals Technology and Applications, vol. 1, John Wiley & Sons, New York, 2003, pp. 99–114, Chapter 9.
[23] S. He, M.M. Mench, S. Tadigadapa, Thin film thermal sensor for polymer electrolyte fuel cells, in: Proceedings of the 206th Meeting of The Electrochemical Society, Microfabricated Systems and

MEMS VII, Honolulu, HI, USA, 3–8 October, 2004, pp. 244–253.
[24] S. Um, C.Y. Wang, K.S. Chen, Computational fluid dynamics modeling of proton exchange membrane fuel cells, J. Electrochem. Soc. 147 (2000) 4485–4493.
[25] S. Dutta, S. Shimpalee, J.W. Van Zee, Numerical prediction of mass exchange between cathode and anode channels in a PEM fuel cell, Int. J. Heat Mass Transfer 44 (2001) 2029–2042.
[26] L.X. You, H.T. Liu, A two-phase flow and transport model for the cathode of PEM fuel cells, Int. J. Heat Mass Transfer 45 (2002) 2277–2287.
[27] D. Natarajan, T.V. Nguyen, A two-dimensional, two-phase, multicomponent, transient model for the cathode of a proton exchange membrane fuel cell using conventional gas distributors, J. Electrochem. Soc. 148 (2001) A1324–A1335.
[28] R. Bradean, K. Promislow, B. Wetton, Transport phenomena in the porous cathode of a proton exchange membrane fuel cell, Numer. Heat Transfer A 42 (2002) 121–138.
[29] A. Rowe, X.G. Li, Mathematical modeling of proton exchange membrane fuel cells, J. Power Sources 102 (2001) 82–96.
[30] M. Kaviany, Principles of Heat Transfer, John Wiley & Sons, New York, 2002, pp. 736–740.
[31] J. Larminie, A. Dicks, Fuel Cell Systems Explained, second ed., John Wiley & Sons, Chichester, West Sussex, UK, 2003, pp. 25–66.
[32] Q. Dong, S. He, M.M. Mench, Dynamic response of current, species, and temperature of PEFCs, in: Proceedings of the 206th Meeting of the Electrochemical Society, Proton Conducting Membrane Fuel Cells IV, Honolulu, HI, USA, 3–8 October 2004, in press.
[33] H.-M. Tong, L.S. Mok, K.R. Grebe, H.L. Yeh, K.K. Srivastava, J.T. Coffin, Effects of parylene coating on the thermal fatigue life of solder joints in ceramic packages, IEEE Trans. Components Hybrid Manuf. Technol. 16 (1993) 571–576.
[34] M.L. Bauccio (Ed.), ASM Engineered Materials Reference Book, second ed., ASM International, Materials Park, OH, 1994, p. 527.
[35] J.R. Davis (Ed.), Metals Handbook, Desk ed., second ed., ASM International, Materials Park, OH, 1998, pp. 652–653.

Biographies

Suhao He was born in Jiangxi, China, in 1979. He obtained his BS and MS degrees from Tsinghua University (PR China) in 2000 and 2002, respectively. He is currently studying for a PhD at the Pennsylvania State University. His first research area was air pollution control. His latest research interests include polymer electrolyte fuel cell science and MEMS. He is a student member of ECS.

Matthew M. Mench is an assistant professor in Mechanical Engineering and the founding director of the Fuel Cell Dynamics and Diagnostics Laboratory at Penn State. Dr. Mench's research interests include fuel cell dynamics and control, transport phenomena, hydrogen and direct alcohol fuel polymer electrolyte fuel cells, and early detection of slow time-scale degradation in fuel cells. Dr. Mench has published articles on topics including hydrogen, direct methanol, and dimethyl ether fuel cell phenomena, solid propellant combustion and stability, and aluminum/liquid oxygen combustion. Dr. Mench is NASA graduate student research program fellow, and was an invited speaker at the 2004 Gordon Research Conference on Fuel Cells. Dr. Mench is a member of the American Society of Mechanical Engineers and the Electrochemical Society.

Srinivas Tadigadapa has been working in the area of microsensors and microactuators for the last 10 years. He completed his PhD from Cavendish Laboratory, Cambridge University, UK in 1994. His research interests include microelectromechanical systems MEMS, novel sensors and actuators, microfluidics, biosensors and biothermodynamics, integrated microsystems, and quantum effects. Dr. Tadigadapa was awarded the Alexander von Humboldt fellowship by the German Government in 1993–1994 during which time he worked on infrared detectors for the NASA CASSINI Space mission. From 1996 to 2000 he worked as the vice president of a MEMS start-up company "Integrated Sensing Systems Inc." in Ann Arbor, Michigan. He has published many technical publications in the area of microsensors, microactuators, their reliability testing and packaging. Dr. Tadigadapa joined as associate professor of Electrical Engineering, at Penn State University in Fall 2000.